

Evaluating the production and exergetic performance of point-of-use reverse osmosis devices for brackish water desalination

Sahil R. Shah*, Amos G. Winter V

Department of Mechanical Engineering, Massachusetts Institute of Technology, Cambridge MA, USA, emails: sahils@mit.edu (S.R. Shah), awinter@mit.edu (A.G. Winter V)

Received 11 December 2022; Accepted 15 June 2023

ABSTRACT

An exergy analysis was conducted to investigate the high specific energy consumption (SEC) of point-of-use reverse osmosis (POU RO) devices. The RO module from one such device was experimentally characterized for desalination of 650, 1,000 and 1,800 mg/L sodium chloride solutions at 70–630 kPa feed pressures. The minimum SEC was 1.54 ± 0.04 kWh/m³, while the maximum second law efficiency and recovery ratio were $1.80\% \pm 0.05\%$ and $24.6\% \pm 0.8\%$, respectively. Losses at the motor, pump, RO element, and flow restrictor respectively accounted for 36%, 25%, 8%, and 29% of the SEC at the intermediate concentration. By highlighting these inefficiencies, we also identified potential avenues for improving the system performance. Recovering brine pressure can decrease SEC significantly. Elevated feed pressures could also decrease SEC and raise recovery ratio but permeate flux would exceed recommended design limits (< 30 L/m²·h), thus increasing fouling risk. The same could be achieved by increasing membrane area provided that the resulting increase in cost and size of the system are acceptable. This work will help guide new developments to decrease the energy consumption of POU RO desalination.

Keywords: Reverse osmosis; Specific energy consumption; Point-of-use; Second law efficiency; Exergy efficiency

1. Introduction

Intermittent and inadequate municipal piped water supply has driven a high reliance on groundwater in Indian cities. Across the country, the World Bank estimates that 85% of drinking needs are met by groundwater [1]. Most of this resource is brackish, with total dissolved solids (TDS) of up to 3,000 mg/L, exceeding the 500 mg/L national standard for drinking purposes [2,3]. To treat this saline supply, many households have turned to point-of-use (POU) reverse osmosis (RO) purifiers.

Even where piped supplies are available, the water can still be regarded as unfit for consumption [4]. Ghosh et al. [5] found that 80% of surveyed Delhi respondents did not consider their municipal water quality to be reliable. This perception has further contributed to the widespread use

of POU RO devices even though desalination may not be required. In the same study, 77%, 44%, and 27% of surveyed high-, middle-, and low-income households used a POU RO purifier.

Significant advances have been made to decrease the energy consumption of RO at a municipal scale [6], but they have not translated to POU systems. The consequence of this disparity is demonstrated in Fig. 1, where we compare the energetic cost of distributed POU desalination to a centralized solution. We estimate that in 2018, POU RO devices in Delhi alone collectively produced 11% as much potable water as one of India's largest municipal seawater desalination plants (Minjur) but consumed 12% as much energy (estimates derived in Appendix A1). This ratio may seem reasonable at first glance, but POU devices primarily treat groundwater with TDS content that is 20–30 times

* Corresponding author.

lower than that of the seawater. Therefore, a lower specific energy consumption can be expected for the POU devices. At the same time, POU systems treat a wide variety of feed-water compositions across the country while lacking the technical supervision found in large-scale plants. Hence, they could be intentionally over-engineered to reliably meet those varying needs.

Operating at recovery ratios of 32% or less [7], today's POU RO systems also withdraw significantly more water per unit volume of treated water than large-scale plants. While the Minjur plant desalinates seawater at a 45% recovery [8], brackish water RO plants can recover 70%–90% from lower-salinity feeds [9–11]. Thus it may be prudent for POU RO systems to process groundwater more economically, since this resource is becoming increasingly scarce in urban India [12]. In fact, the National Green Tribunal (NGT) of India is advocating for a ban on POU RO in places where the source water TDS does not exceed 500 mg/L, and enforcing a minimum 60% recovery in places where they can be used.

Adoption of POU RO purifiers has risen since 2017 due to growth in India's middle-class income, and poor water quality in many parts of the country. Without technological upgrades, environmental impact can be estimated to have scaled with forecasted sales growth (16%/y [13]). Then, POU devices in Delhi are expected to consume one-fourth the energy of Minjur by 2023 (Fig. 1). Market research also suggests that there is a lack of product differentiation among competing units [13]. Beyond the addition of more pre- and post-filtration stages, the core architecture of RO modules has remained largely unchanged since their introduction to the Indian market in 1999. Therefore, in addition to environmental and legislative drivers, there is also an economic incentive to innovate improved solutions.

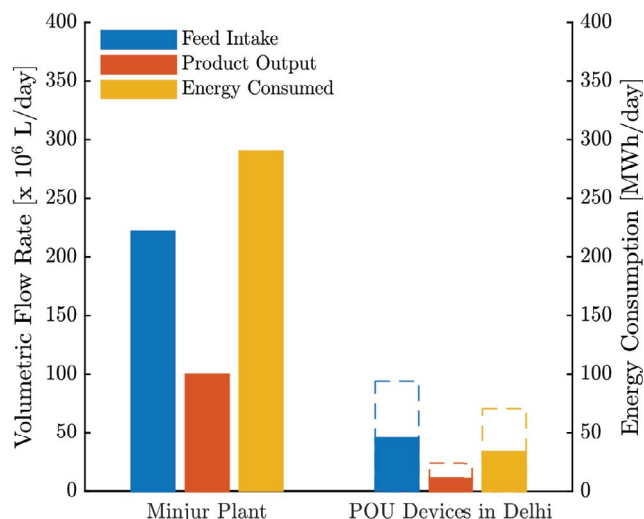


Fig. 1. Energy and water consumption comparison between all point-of-use (POU) RO devices in Delhi in 2018 to one of India's largest seawater desalination plants, Minjur. The POU devices produce an equivalent of 11% of Minjur's capacity but consume 12% as much energy (solid). Their collective energy consumption is projected to double by 2023 due to increased adoption (dashed).

The objective of this work is to experimentally characterize the performance of a POU RO system and conduct an exergy analysis to identify key inefficiencies. In doing so, we hope to catalyze new developments in POU RO desalination that address the discrepancies illustrated in Fig. 1.

Prior studies evaluating POU RO desalination have not investigated the energy losses within such a system. Elfil et al. [14] performed a techno-economic analysis on the use of POU RO devices in Tunisia, which encompassed an evaluation of the scaling propensity and recovery ratio for different feed water compositions and temperatures. They concluded that the treatment cost was 11–30 times greater than can be achieved with large scale plants when water, energy consumption, and membrane replacement are considered. However, they did not quantify the inefficiencies underlying this large difference. To specifically address the low recovery ratio, Thampy et al. [15] proposed hybridization with an electro dialysis process for POU desalination and demonstrated that recovery could be raised to 50%–60% for 2,000–4,000 mg/L feeds. The energy consumption of the proposed process was 8–10 kWh/m³, which equates to approximately thrice the 2.9 kWh/m³ consumption of the Minjur seawater desalination plant in Fig. 1. By analyzing the RO process for POU systems in detail, we aim to identify other strategies for improving recovery with lower energetic penalties.

2. General description of POU RO systems

Fig. 2 shows an example of the filtration steps within a POU RO system. The core RO process highlighted in gray is the same across different products, but pre- and post-treatment steps may vary. This process contains a booster pump, RO element, and flow restrictor in the configuration shown. The highlighted subsystem is the focus of this study, as it is the largest energy consumer in the POU system. In this

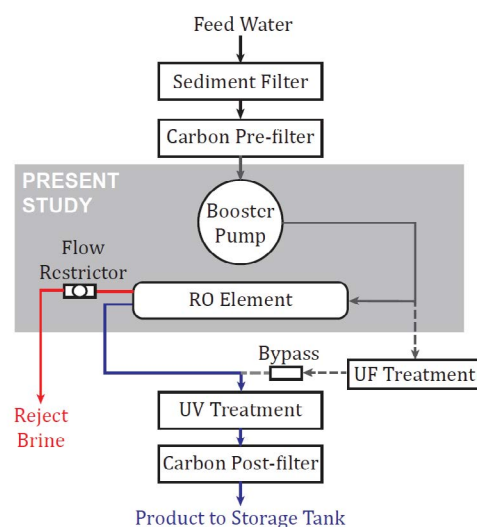


Fig. 2. General configuration of POU desalination systems includes a reverse osmosis stage surrounded by other treatment. The RO module of present interest is fixed (highlighted in gray), while the type of pre- and post-filtration may vary across different POU RO products.

work, we tested the RO subsystem from a Dr. Aquaguard Magna Purifier (Bengaluru, Karnataka, India) (Eureka-Forbes) [16] which consumes 24 W of the 35 W total electrical power consumption. The remainder is consumed by the ultraviolet (UV) lamp.

Incoming water is sufficiently pressurized for the pre-filtration, but the booster pump provides the pressure for RO desalination and post-filtration. Diaphragm pumps are typically used in this application because they are inexpensive. The pump assembly evaluated in this study was manufactured by CSE Company Ltd., (Siheung-si, Gyeonggi-do, South Korea), (Model CS-0580Q-AQ), but the observed efficiency matches POU RO pumps from other manufacturers. For example, from the data provided by Aquatec (Irvine, California, USA) (Model 8800) and EFlow (Model ZS-ARON75G) for pumps providing similar pressure and flow rate performance, the peak efficiencies are 47% and 34%, respectively. These values are comparable to the peak efficiency of $45\% \pm 2\%$ observed for the pump evaluated in this work. Thus, our findings regarding the impact of pump efficiency are relevant to other POU RO devices.

Spiral-wound POU RO elements are also commodity items manufactured in standard sizes. The element evaluated in this work was manufactured by Infinite Water Solutions Ltd., (Dehradun, Uttarakhand, India), (HTFC75 NANO). It has a nominal permeate production capacity of 12 L/h (75 gal/d) and matches the pressure vs. flow performance of equivalent Pentair (TLC-75 [17]) and DOW (FilmTec™ BW60-1812-75 [18]) products. This agreement provides further assurance that while only one POU product was evaluated here, the results can be generalized to other devices.

In some POU RO systems, a bypass valve is used to reintroduce salinity to the product stream. The extent to which this valve is opened depends on user preferences. In this work, we assume that there is no mixing of the feed and product to provide an upper bound on the system's second law efficiency.

Finally, it is worth noting that testing was performed on an RO element that was previously unused. Furthermore, the POU system implements a continuous flow configuration (Fig. 2) but is intermittently operated under normal use. Membrane permeability coefficients are known to decrease with sustained use [19], and particularly with intermittent operation [20,21], causing energy consumption to consequently increase, and production rate to decrease. It follows that the results presented here represent the upper bound of energetic and production performance for today's POU RO systems.

3. Experimental methods and data

We first experimentally evaluated the RO subsystem from a POU purifier. Power consumption, rate of desalinated water production, and recovery ratio were measured to quantify performance (Section 3.1 – RO system evaluation). To understand the conversion from electric to hydraulic energy, the motor was detached from the pump and evaluated independently on a dynamometer (Section 3.2 – Pump motor characterization). In this section, we detail both experiments.

3.1. RO system evaluation

A diaphragm booster pump and an encapsulated spiral-wound RO element were obtained from a Dr. Aquaguard Magna Purifier (Eureka-Forbes) [16], and fitted to a test setup (Fig. 3) to characterize performance. Experimental measurements of flow rates, conductivities, pressures, and power draw, were taken at three different feed concentrations (approximately 650, 1,000 and 1,800 mg/L of sodium chloride), and feed pressures ranging between 70 to 630 kPa. Feed solutions, at all three concentrations, were prepared by adding lab-grade sodium chloride (Sigma-Aldrich, St. Louis, Missouri, USA) to distilled water whose initial conductivity was ~ 2 $\mu\text{S}/\text{cm}$. The data collected in

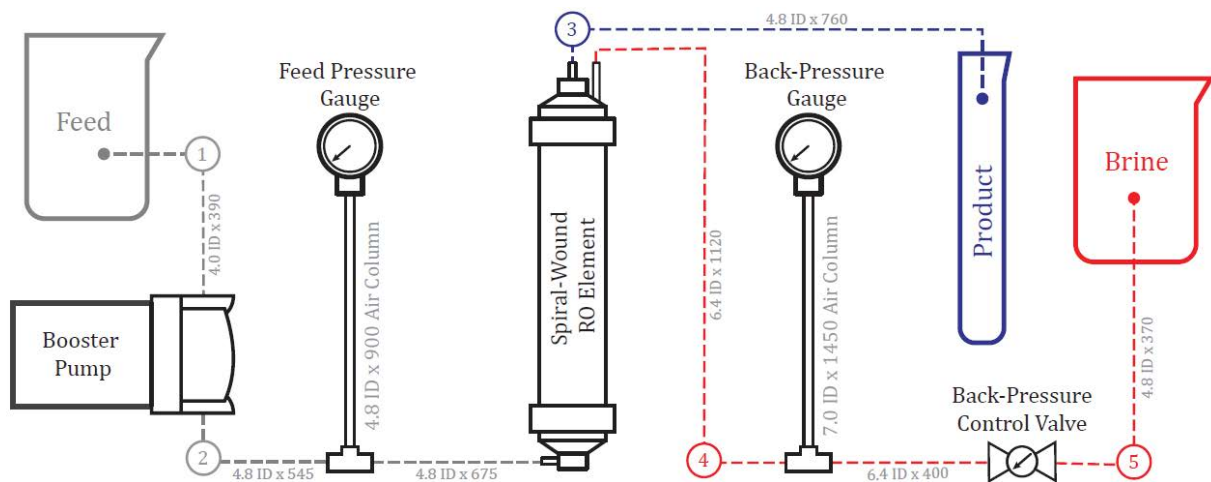


Fig. 3. This is a schematic of the experimental set-up. It incorporated a spiral-wound RO element and booster pump from a POU RO purifier. Flow rates and concentrations of brine and product were measured for varying feed concentrations and pressures. Streams are numbered 1–5 and referenced in the exergy analysis (Section 4 – Exergy analysis). The air columns attenuated pressure fluctuations originating at the diaphragm booster pump. Tubing lengths and internal diameters (mm) are provided for pressure drop calculations.

these tests is provided in Table A2. Real Indian groundwater contains additional salts whose concentrations vary both geographically and seasonally. However, the least work of separation results calculated for the model sodium chloride solutions employed in this study are similar to those for more complex groundwater matrices of equal molalities [22].

The feed-pressure was adjusted using a control valve fitted to the reject line in approximately 70 kPa increments up to the maximum pump pressure of 630 kPa. This pressure was measured using a dial gauge (Aschroft 1005, Stratford, Connecticut, USA). An additional pressure gauge (Dwyer Instruments, Michigan City, Indiana, USA) was fitted downstream of the RO element, so that pressure drop across the element could be quantified. Pressure fluctuations from the diaphragm pump were attenuated by the air columns that occupied the sensing tubes to the gauges.

After setting the feed-pressure for each test, the system was allowed to achieve steady operation over a minimum of 60 s, which is approximately six times the feed residence time within the RO element. At the end of this period, the pump's DC current draw was recorded from the adjustable power supply (Dr. Meter PS-305DM, Shenzhen Thousandshores Technology Company, Shenzhen, China). Then, brine and permeate were collected over an additional 45–60 s duration in a 2 L beaker and a 250 mL measuring flask, respectively. The collected masses of brine and product, measured using a weigh scale (Ohaus Scout Pro, Parsippany, New Jersey, USA), were subsequently used to estimate flow rates. Conductivities of the feed, brine, and product were measured at the end of each test using a handheld conductivity meter (Myron L Company, Ultrameter II, Carlsbad, California, USA). The same device was also used to measure feed temperature, which remained between 22°C–25°C through all tests.

Upon completing the tests, the RO element was unwound so that membrane and spacer dimensions could be measured. These data are provided to facilitate future modeling and design efforts (Table 1).

3.2. Pump motor characterization

The torque-speed relationship of the brushed DC motor used in the booster pump was measured using a dynamometer [24], at its 24 V rating (Fig. 4). The speed of the absorber was controlled through 60 steps, from 0 to the motor's

Table 1
RO element – membrane and spacer dimensions

Parameter	Value
Membrane width within glue strips, W	1.30 m
Membrane length within glue strips, L	0.19 m
Total membrane area ^a , $S = 2LW$	0.494 m ²
Feed spacer filament diameter	0.216 mm
Feed spacer filament spacing	1.75 mm
Feed spacer filament angle ^b	90°
Permeate spacer height	0.254 mm

^aTransport occurs across both walls of the permeate channel;

^bFilament angle is defined as in Koutsou et al. [23].

95 rad/s maximum. The motor speed was allowed to settle after each speed command before torque, speed, and current were sampled at 150 Hz for 4 s and averaged. These measurements were used to fit motor constants (Table 2) and derive the motor's output power and efficiency curves. The methodology and raw data is provided in Appendix A3.

4. Exergy analysis

An exergy analysis was conducted to quantify the inefficiencies in the system. An overview of the methodology and key equations are presented here to guide the reader's understanding of the work. However, a more complete description of the exergy concept and its application to analyzing desalination systems can be found in Mistry et al. [25]. The total work of separation \dot{W}_{sep} (W) is represented by the sum.

$$\dot{W}_{sep} = \dot{W}_{least} + \sum_i \dot{\Xi}_{d,i} \quad (1)$$

where \dot{W}_{least} (W) is the least work of separation at a finite recovery ratio, and each $\dot{\Xi}_{d,i}$ (W) term represents the exergy destroyed by each component i due to irreversible operation. Normalizing by the volumetric rate of desalinated water production Q_p (m³/s) allows the specific energy consumption SEC (J/m³) to be represented as the sum of contributions from the least work and the losses.

$$SEC = \frac{\dot{W}_{sep}}{Q_p} = \frac{1}{Q_p} \left(\dot{W}_{least} + \sum_i \dot{\Xi}_{d,i} \right) \quad (2)$$

For the present system, the work of separation is the electrical energy supplied to the motor. Therefore,

$$\dot{W}_{sep} = IV \quad (3)$$

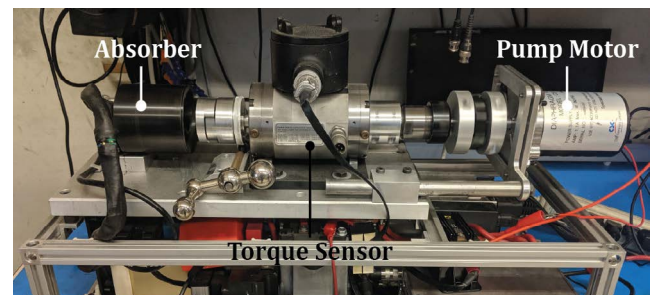


Fig. 4. The torque-speed characteristics, and efficiency of the pump's motor were measured on a dynamometer. The absorber controls the speed of the motor, while the torque sensor measures torque output from the motor at that speed.

Table 2
Empirically fitted motor constants

Parameter	95% C.I.
Velocity constant, k_v (V-s/rad)	0.260 ± 0.003
Torque constant, k_t (N-m/A)	0.228 ± 0.001
Winding resistance, R_m (Ohms)	7.1 ± 0.2

where V (V) is the voltage supplied to the motor, and I (A) is the measured current. Then, the second law efficiency of the system η_{II} is:

$$\eta_{II} = \frac{\dot{W}_{\text{least}}}{IV} \quad (4)$$

Each exergy destruction term is calculated from:

$$\dot{\Xi}_{d,i} = \sum_{\text{in-out}} \dot{\Xi}_{w,i} + \sum_{\text{in-out}} \dot{\Xi}_{s,i} \quad (5)$$

indicating that exergy flows can relate to both work $\dot{\Xi}_w$ or process streams $\dot{\Xi}_s$ (W). For process streams, the specific exergy per unit mass ξ (J/kg) is defined as:

$$\xi = \underbrace{(h - h^*)}_{\text{enthalpy}} - T_0 \underbrace{(s - s^*)}_{\text{entropy}} + \sum_i^n w_i \underbrace{(\mu_i^* - \mu_{i,0})}_{\text{chemical potential}} / M_i \quad (6)$$

where h , s , w_i , μ_i , and M_i are the specific enthalpy (J/kg), specific entropy (J/kg·K), the mass fraction of species i of n , its chemical potential (J/mol), and its molar mass (kg/mol). Properties with the superscript * are evaluated at the temperature T_0 (K) and pressure P_0 (Pa) of the environment, but at the same composition as the stream of interest (restricted dead state). However, properties with the subscript 0 are evaluated at the temperature, pressure, and composition of the environment (global dead state).

Applying these expressions, we derived the exergy destruction and exergy efficiency for each component. The equations are summarized in Table 3, while details are provided in the following subsections. The primary assumptions include:

- (i) All streams are at the temperature of the feed solution. This is a common assumption for the analysis of RO systems since it is a pressure-driven process. It follows that the enthalpy differences in Eq. (6) may only arise due to changes in pressure.
- (ii) The disposal of concentrated brine is not treated as lost exergy. Instead, the least work is defined as the

minimum work to separate the feed stream into concentrated and diluted streams, at a finite recovery ratio. This definition allows direct comparison with exergy efficiencies of brackish water RO plants reported in literature. When the disposal of concentrated brine is treated as lost exergy, the maximum second law efficiency drops from $1.80\% \pm 0.05\%$ (Section 5.1 – Specific energy consumption) to $1.61\% \pm 0.05\%$ while other conclusions are unaffected. For a detailed discussion on the difference between the two approaches, Qureshi and Zubair [26] and Mistry et al. [25] are recommended.

- (iii) The solution is treated as incompressible. Therefore, entropy has no pressure dependence.
- (iv) The feed temperature, composition, and atmospheric pressure specify the global dead state for each test.
- (v) The literature provides different definitions for the exergy efficiency of the RO element. We apply the definition provided by Blanco-Marigorta et al. [27], whereby the RO element is evaluated on its ability to exchange physical exergy for chemical exergy.

4.1. Least work of separation

The least work of separation is the difference in chemical potential energy of the product and brine streams, relative to the feed. From the derivation provided in Appendix A4:

$$\begin{aligned} \dot{W}_{\text{least}} = & 2\dot{m}_{\text{H}_2\text{O},p}RT \left[-b_p\phi_p + b_f\phi_f + b_p \ln \left(\frac{\gamma_p b_p}{\gamma_f b_f} \right) \right] \\ & + 2\dot{m}_{\text{H}_2\text{O},b}RT \left[-b_b\phi_b + b_f\phi_f + b_b \ln \left(\frac{\gamma_b b_b}{\gamma_f b_f} \right) \right] \quad (7) \end{aligned}$$

The mass flow rate of water in each stream $\dot{m}_{\text{H}_2\text{O}}$ (kg/s) and the associated molality of sodium chloride b (mol/kg) were calculated from the raw results using the procedure outlined in Appendix A5. R is the gas constant (J/mol·K), T is temperature (K), and the product, brine, and feed streams are differentiated by subscripts p , b , and f , respectively. The osmotic coefficients ϕ and mean molal activity coefficients γ were taken from Partanen's work [28].

Table 3
Equations for quantifying each component's exergy destruction and exergy efficiency

Component, i	Exergy destruction, $\dot{\Xi}_{d,i}$	Exergy efficiency, ϵ_i
Full system	$IV - \dot{W}_{\text{least}}$ (Eq. (7) for \dot{W}_{least})	$\dot{W}_{\text{least}} / IV$
Pump, motor	$IV - \frac{k_T}{k_V} (IV - I^2 R_m)$	$\frac{k_T}{k_V} \left(1 - \frac{IR_m}{V} \right)$
Pump, hydraulics	$\frac{k_T}{k_V} (IV - I^2 R_m) - P_f Q_f$	$P_f Q_f / \left(\frac{k_T}{k_V} (IV - I^2 R_m) \right)$
RO element	$P_f Q_f - P_b Q_b - \dot{W}_{\text{least}}$	$\dot{W}_{\text{least}} / (P_f Q_f - P_b Q_b)$
Flow restrictor	$P_b Q_b$	–

Note that at the limit of infinitesimal recovery ($b_b = b_p$) and pure water production ($b_p = 0$), Eq. (7) simplifies to:

$$\dot{W}_{\text{least}} = \frac{\dot{m}_{\text{H}_2\text{O},p}}{\rho_{\text{H}_2\text{O}}} (2RTb_f\phi_f\rho_{\text{H}_2\text{O}}) = Q_p\pi_f \quad (8)$$

where π_f (Pa) is the feed osmotic pressure.

4.2. Pump motor

As specified earlier, the exergy input to the motor is the electrical power (IV). Exergy output from the brushed DC motor $\dot{\Xi}_{\text{out},m}$ (W) is mechanical power, given by the product of torque τ (N-m) and rotational speed ω (rad/s). Since these quantities could not be directly measured during operation of the pump, the exergy output was estimated from:

$$\dot{\Xi}_{\text{out},m} = \tau\omega = k_T I \left(\frac{V}{k_V} - \frac{R_m}{k_T k_V} \tau \right) = \frac{k_T}{k_V} (IV - I^2 R_m) \quad (9)$$

using fitted motor constants from dynamometer testing (Table 2).

4.3. Pump hydraulics

The two exergy inputs are related to the mechanical power from the motor and the feed stream (Stream 1 in Fig. 3). Since this stream defines the dead state properties, $\dot{\Xi}_1 = 0$. Neglecting the dependence of entropy on pressure (Assumption 3), the exergy flow associated with output Stream 2 is:

$$\dot{\Xi}_2 = P_f Q_f \quad (10)$$

due to the elevated feed pressure P_f (Pa). The average feed volumetric flow rate Q_f (m³/s) for each test can be estimated from the measured product and brine mass flow rates m using:

$$Q_f = \frac{1}{\rho} (\dot{m}_p + \dot{m}_b) \quad (11)$$

where ρ (kg/m³) is taken to be the density of the solution at the dead state. Appendix A5 outlines how the solution density, molality, and molarity were correlated to the conductivity measurements.

4.4. RO element

The exergy input of the feed stream $\dot{\Xi}_2$ is given in Eq. (10), while the brine and product streams form the exergy outputs. Applying Eq. (6) to the product (Stream 3), we find that the exergy is only related to the chemical potential difference since the temperature and pressure are equal to those of the dead state. Then, applying the same substitutions as in Appendix A4:

$$\dot{\Xi}_3 = 2\dot{m}_{\text{H}_2\text{O},p} RT \left[-b_p\phi_p + b_f\phi_f + b_p \ln \left(\frac{\gamma_p b_p}{\gamma_f b_f} \right) \right] \quad (12)$$

The brine leaving the RO element (Stream 4) is pressurized to P_b (Pa). Accounting for both the enthalpy and chemical potential difference,

$$\dot{\Xi}_4 = P_b Q_b + 2\dot{m}_{\text{H}_2\text{O},b} RT \left[-b_b\phi_b + b_f\phi_f + b_b \ln \left(\frac{\gamma_b b_b}{\gamma_f b_f} \right) \right] \quad (13)$$

where Q_b is the brine volumetric flow rate.

Note that summing the exergy outputs from the RO element and substituting Eq. (7) gives the result:

$$\dot{\Xi}_3 + \dot{\Xi}_4 = \dot{W}_{\text{least}} + P_b Q_b \quad (14)$$

The least work of separation appears in this expression because the separation process occurs within the RO element.

4.5. Flow restrictor

The restrictor depressurizes the brine stream. Therefore, the exergy of Stream 5 is simply altered from that of Stream 4 [Eq. (13)] to:

$$\dot{\Xi}_5 = 2\dot{m}_{\text{H}_2\text{O},b} RT \left[-b_b\phi_b + b_f\phi_f + b_b \ln \left(\frac{\gamma_b b_b}{\gamma_f b_f} \right) \right] \quad (15)$$

5. Results and discussion

The exergy analysis outlined above was conducted using the measured data to estimate second law efficiency, high-light significant losses, and suggest areas for improvement.

5.1. Specific energy consumption

SEC is plotted against feed pressure and feed concentration (Fig. 5). Tests where the applied pressure only marginally exceeded the osmotic pressure were excluded given that the permeate production rate was far below the RO element's nominal 12 L/h specification. Likewise, tests conducted at 630 kPa were excluded because brine flow was almost fully choked, and the pump was close to stalling. Between these limits, a minimum measured specific energy consumption of 1.54 ± 0.04 kWh/m³ was obtained at the lowest feed concentration of 650 mg/L, and the highest feed pressure of 560 kPa.

SEC increased with feed concentration as expected, because permeate flux decreases when a constant pressure is applied against increasing feed osmotic pressures. At the same 560 kPa pressure, the SEC was 1.63 ± 0.05 kWh/m³ and 1.99 ± 0.06 kWh/m³ for the intermediate and high feed concentrations, respectively. Fig. 5 also shows SEC decreasing with increasing feed pressure. This behavior is less intuitive and examined more closely in the following subsection.

The stacked bars (Fig. 5) present a breakdown of SEC into the least work of separation and accumulated losses due to exergy destruction at the individual components, per Eq. (2). This breakdown indicates that the booster pump

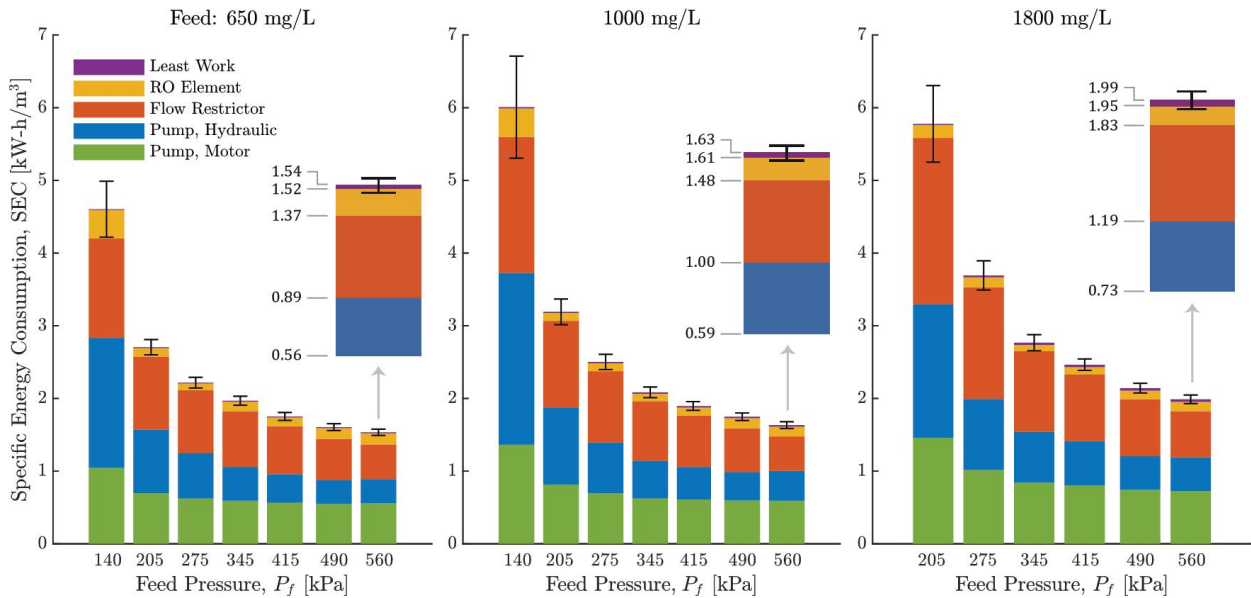


Fig. 5. The measured specific energy consumption (SEC) is plotted for varying feed pressures at the three different feed concentrations. It is represented as the sum of the least work of separation and the accumulated exergy destruction at components, all normalized by the volumetric production rate. The total bar height at each feed pressure is the SEC, while the ratio of the purple bar height to total height is the system's second law efficiency (quantified in Fig. 7). Error bars represent propagated measurement uncertainty.

assembly (motor and pump, together), followed by the discharge of pressurized brine, contributes the greatest losses in the system. These losses respectively account for 36%, 25%, and 29% of the measured SEC at 1,000 mg/L and highest feed pressure. Note that the motor is the most upstream component in the system that was analyzed; hence, it powers all downstream processes. Downstream inefficiencies therefore have a compounded effect on the exergy destruction at the motor. Consider the scenario where exergy destruction caused by brine depressurization at the flow restrictor was lowered. Then the motor would be required to output less power to maintain the same permeate production rate, concurrently generating smaller losses. It follows that reducing, or recovering, the brine pressure can significantly decrease the system SEC.

Losses at the RO element account for only 8% of the system SEC, but a comparison of exergy efficiencies reveals that it is the least efficient component (Fig. 6). Appearing contradictory at first glance, these two results are in fact consistent because the RO element consumes only a small fraction of the hydraulic power generated by the pump. The remainder is dissipated by the flow restrictor. Therefore, permeation losses, viscous losses, and losses due to concentration polarization within the RO element are small when compared to losses at the other components under the intended system operation. Thus, improving the efficiency of the RO element alone will not decrease SEC significantly.

5.2. Effect of feed pressure on production rate, recovery, and SEC

The system's maximum measured second law efficiency was $1.80\% \pm 0.05\%$ at the 1,800 mg/L feed and maximum pressure (Fig. 7). It was described previously that one way to improve this efficiency is to minimize exergy destruction

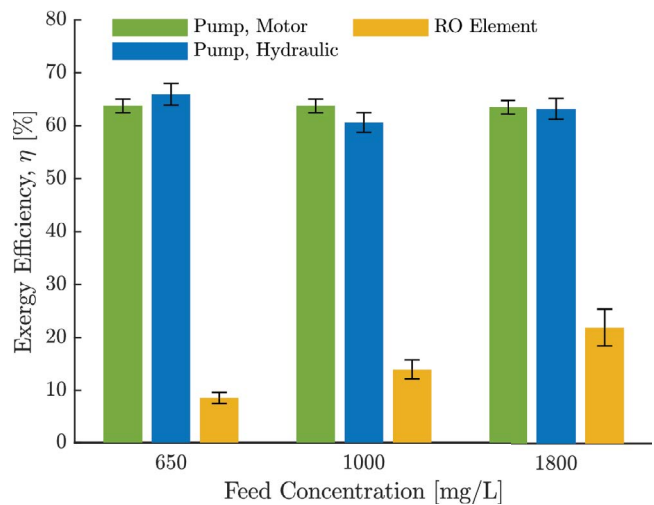


Fig. 6. Exergy efficiencies of the individual components are plotted against feed concentration, for operation at 560 kPa feed pressure. The efficiency definitions are summarized in Table 3. The flow restrictor is a purely dissipative element ($\eta = 0$) and is therefore excluded here. Error bars represent the root mean square of measurement uncertainty and standard deviation.

at the flow restrictor via pressure recovery. Another potential solution is to raise feed pressure. The observed decrease in SEC with increasing feed pressure (Fig. 5) is explained by two mechanisms.

- (1) Fig. 8 shows that a minimum 5 W are consumed by the pump assembly before any water is desalinated from a 1,000 mg/L feed. This quantity represents the sum of frictional dissipation at no-load and the power required

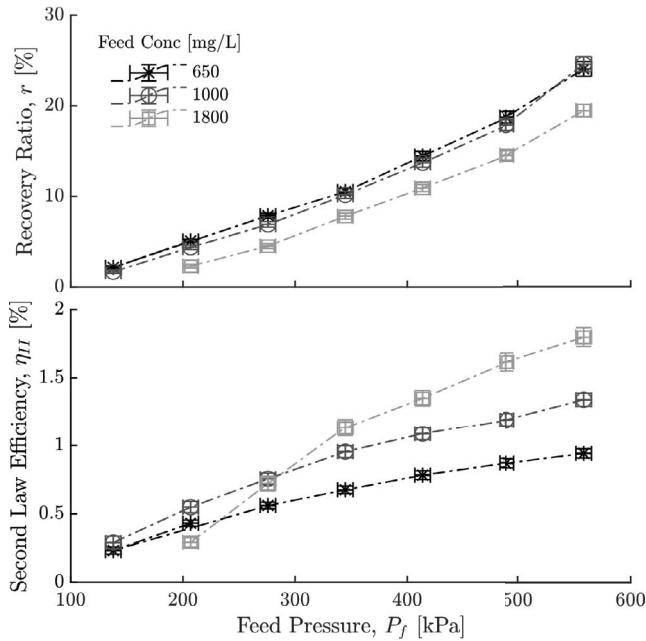


Fig. 7. Recovery ratio and system efficiency both increased with feed pressure. The maximums were $24.6\% \pm 0.8\%$ and $1.80\% \pm 0.05\%$, respectively. Error bars represented propagated measurement uncertainty.

to overcome the feed osmotic pressure. As feed pressure rises, this minimum loss becomes distributed over an increasing product flow rate, causing SEC to decrease.

- (2) Recovery grows with feed pressure (Fig. 7), causing brine pressurization to have a decreasing impact on SEC. To see this relationship, consider exergy destruction at the flow restrictor (Table 3), and neglect pressure drop through the RO feed channel, so that brine pressure equates feed pressure ($P_b \approx P_f$). Then, the respective contribution of brine depressurization to SEC is approximately:

$$\text{SEC}_{\text{tr}} \approx \frac{P_f Q_b}{Q_p} = P_f \underbrace{\left(\frac{1}{r} - 1 \right)}_{\text{II}} \quad (16)$$

where r is the recovery ratio. The above expression indicates that for the same recovery, a doubling of the feed pressure would cause SEC to also double. However, it can be deduced from Fig. 7 that the same increase in feed pressure causes recovery ratio to increase by a larger multiple. It follows, term II of Eq. (16) decays faster than term I grows, causing a net decrease in SEC with rising feed pressure.

The trends observed in Fig. 5 support the analysis that raising feed pressure will decrease losses at the pump assembly (green and blue bars) and flow restrictor (red bar) via the mechanisms detailed above, albeit at a diminishing rate. However, the reverse occurs at the RO element (orange bar). At low permeate flux, when brine flow rates are highest, energy consumption is dominated by pressure drop across the element's feed channel. At higher permeate fluxes,

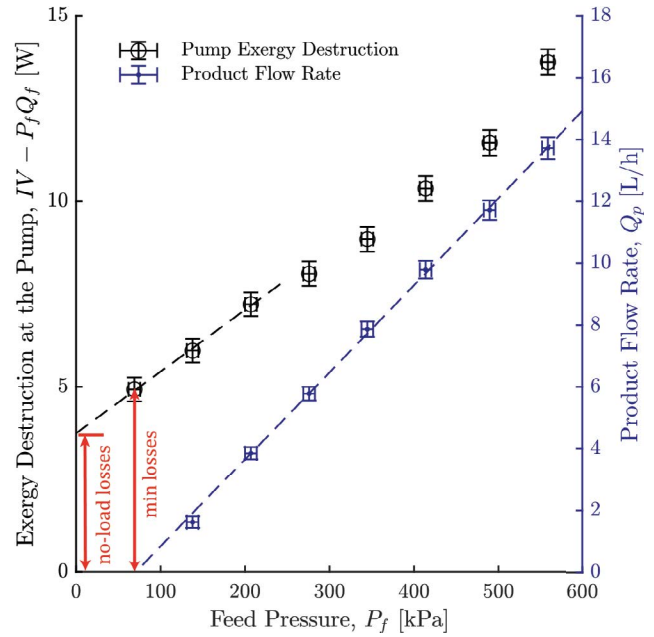


Fig. 8. Exergy destruction at the pump, and product flow rate, are plotted against feed pressure. The x -intercept of the flow rate vs. feed pressure plot is the feed osmotic pressure π_f . Above this pressure, the flow rate is linear with the over-pressure ΔP_f . A minimum of 5 W is dissipated by friction at the pump before any desalinated water is produced. Results are plotted for the 1,000 mg/L feed, and error bars represent propagated measurement uncertainty.

when the membrane is operated as intended, this pressure drop decreases so that the brine pressure P_b approaches the feed pressure P_f (Table A2). In this regime, the losses at the element contributing to SEC are found to be proportional to permeate flux J_w (Fig. 9) such that:

$$\text{SEC}_e \approx \frac{1}{A_m} J_w \quad (17)$$

The proportionality constant is the effective membrane permeability, A_m . The slope of the product flow rate vs. pressure curve (Fig. 8), normalized by membrane area (Table 1), suggests that $A_m = 5.7 \pm 0.2 \text{ L/m}^2\text{-h}\cdot\text{bar}$. This value is lower than the membrane's true permeability because it incorporates the resistance that arises from concentration polarization. The calculated element SEC closely matched this expected linear relationship (Fig. 9), and the small systematic underprediction is explained by the neglected pressure drop in the brine stream. It follows that since permeate flux is proportional to the feed pressure, an increase in feed pressure will generate a linear increase in losses at the RO element.

Thus, for the POU system of present interest, we have shown that specific exergy destruction at the RO element grows linearly with increasing feed pressure, while at the pump and throttle it decays with feed pressure. Since exergy destruction at the pump assembly and throttle outweigh those at the RO element, local increases in feed pressure

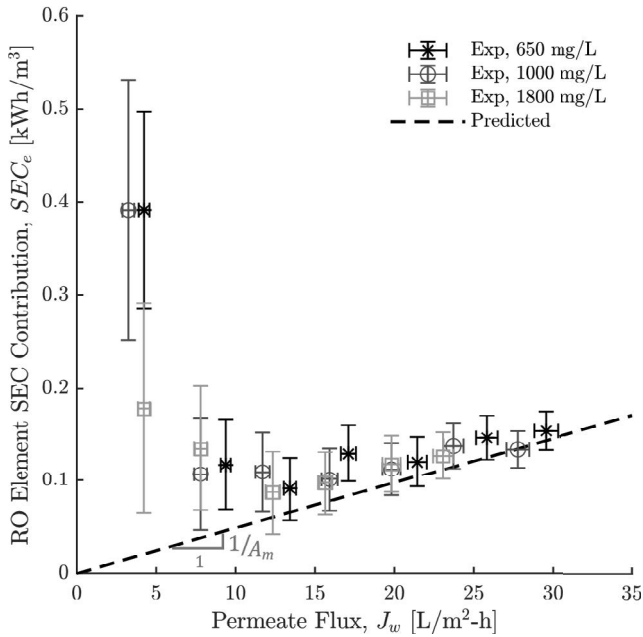


Fig. 9. The SEC contribution due to exergy destruction at the RO element is plotted against permeate flux J_w . Viscous pressure drop through the brine channel dominates at low flux, while pressure drop due to membrane permeation dominates at high flux. The latter process is expected to produce a linear trend with a slope corresponding to the inverse of the effective membrane water permeability coefficient, $A_m = 5.7 \pm 0.2$ L/m²-h-bar. Error bars represent propagated measurement uncertainty.

are therefore expected to produce a net decrease in SEC. An extrapolation of the SEC vs. feed pressure trend in Fig. 5 reinforces this expectation. Furthermore, it is seen that recovery ratio, production rate, and second law efficiency also improve simultaneously with increasing feed pressure (Figs. 7 and 8). This synergy could be potentially exploited to improve system performance across-the-board.

There are however two constraints that may limit the extent to which feed pressure may be increased:

- Maximum permeate flux: Membrane manufacturers recommend an average permeate flux of 23–31 L/m²-h for brackish water desalination to minimize fouling and prevent mechanical damage [29,30]. At the highest pressures, the 30 L/m²-h flux for the present system approaches the recommended upper bound (Fig. 9). As a result, accelerated fouling or membrane damage may be one barrier to raising feed pressure beyond the present range.
- Maximum element pressure: Another barrier to raising feed pressure is the maximum pressure rating: 830 kPa for the present RO element. We did not investigate failure mechanisms that prevent operation at higher pressures. However, other manufacturers provide products that are rated to higher pressures: 1,035 kPa for both FilmTec™ [18] (DOW) and NanoH₂O™ (LG) products [31]. Therefore, it appears feasible for POU systems to access the energetic benefits enabled by higher feed pressures.

5.3. Effect of element membrane area on SEC

To circumvent RO element pressure and flux limitations, a third strategy to decrease SEC is by increasing the membrane area usage. Membrane area can be increased by using a larger RO element containing more membrane surface, adding a second RO stage, or recirculating the brine in a batch or semi-batch process [32–35] so that the same membrane area is reused several times. In all cases, designers would be required to balance the efficiency gains with increased capital cost.

An increased membrane usage can enable specific energy savings through one of two pathways:

- (1) One could maintain the same production rate and recovery but decrease the average flux through the membrane. By acknowledging that the flux J_w is the ratio of the volumetric production rate Q_p to the membrane area S , Eq. (17) can be expressed as:

$$SEC_e \approx \frac{1}{A_m} J_w = \frac{1}{A_m} \frac{Q_p}{S} \quad (18)$$

Doubling the membrane area, without changing production rate, could therefore halve the SEC contribution related to losses at the RO element.

- (2) A different approach involves raising production rate at the same permeate flux. In this case, the losses at the element would remain unchanged. However, Eq. (16) indicates that the subsequent increase in recovery (assuming an unchanged feed flow rate) would lower brine depressurization losses at the flow restrictor.

As discussed in Section 5.2 – Effect of feed pressure on production rate, recovery, and SEC, the losses at the flow restrictor outweigh those at the RO element for this system. Therefore, the second of these two approaches would yield greater SEC savings. Since this approach relies on increasing the recovery of the system, the extent to which it is effective will depend on the chemistry of the water being desalinated and the brine's propensity to scale.

5.4. Pump performance

Summing electric and hydraulic losses, we found that losses at the booster pump assembly contribute most significantly to the system SEC (Fig. 5), in part because it is the most upstream component of the process. Thus, SEC could be decreased substantially by raising the efficiency of the constituent pump and motor. The combined efficiency of the assembly η_p peaked at 45% \pm 2% and remained relatively flat over a wide operating range (Fig. 10). At this peak, the motor electrical efficiency η_m was 70% \pm 1%, giving an estimated pump hydraulic efficiency η_h ($=\eta_p/\eta_m$) of 64% \pm 1%. These efficiencies are acceptable given the small size of the pump, and it would therefore be difficult to increase them substantially.

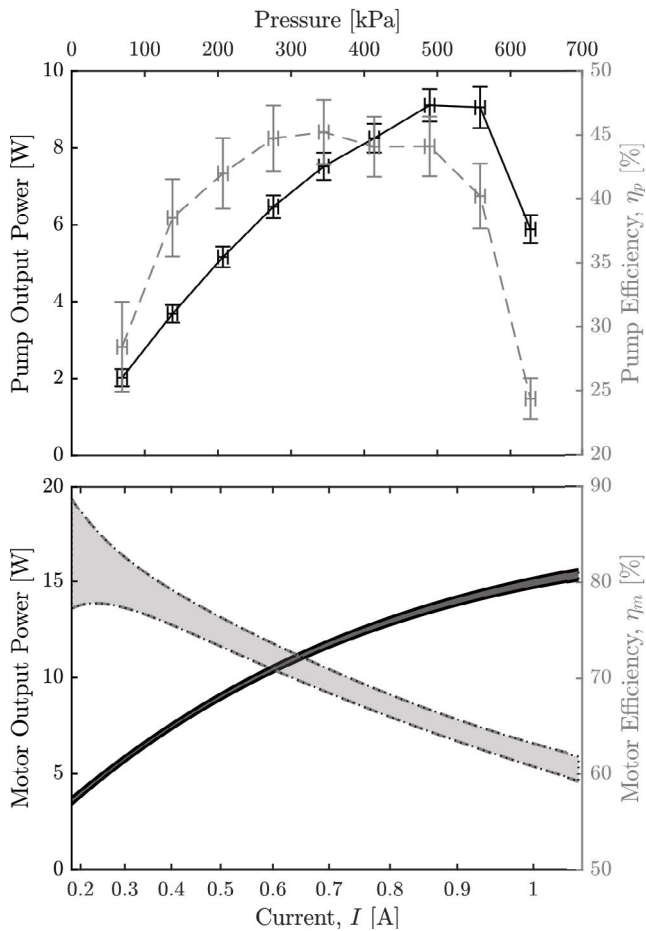


Fig. 10. The measured pump (motor and hydraulic) power and efficiency are plotted against feed pressure (top). The 95% prediction interval for motor power and efficiency are represented by the shaded region for the same operating range, by correlating pump pressure to current draw (bottom). The combined pump efficiency peaked at $45\% \pm 2\%$, while the motor alone is most efficient at low output powers where small currents decrease ohmic losses. Error bars in the top graph represent measurement uncertainty.

6. Conclusions

Point-of-use reverse osmosis (POU RO) devices have enabled households to produce drinking water from saline water supplies where municipal piped water has been unreliable or distrusted. However, they are inefficient when compared to large-scale processes, with respect to both recovery ratio and SEC. In this work, an RO element and corresponding pump from one such POU device was experimentally evaluated at varying feed pressures of 70–630 kPa and three sodium chloride concentrations: 650, 1,000 and 1,800 mg/L. A subsequent exergy analysis using the experimental results indicated a maximum second law efficiency of $1.80\% \pm 0.05\%$ for the system, and a minimum SEC of 1.54 ± 0.04 kWh/m³.

Three directions for decreasing SEC were identified. First, the depressurization of brine at the flow restrictor accounts for 29% of the specific energy consumption. Recovering this energy will also decrease losses at the upstream pump.

The second suggestion involves raising feed-pressure to increase recovery ratio. This approach would decrease exergy destruction due to brine throttling and distribute pump frictional losses over greater volumes of produced water. However, since the 30 L/m²-h permeate flux at the highest pump pressures already approaches the element's maximum specification, operation at even higher pressures may increase fouling propensity. To bypass this limitation, a third approach involves maintaining the same feed pressures but either increasing membrane area by adding membrane elements in series or recirculating the feed in batch operation.

The spiral-wound RO element had an exergy efficiency of 8.6%–21.9% at maximum pressure, when system SEC was lowest for each feed. Losses were primarily caused by over-pressure due to concentration polarization and permeation through the membrane. These losses account for only 8% of the system's SEC at the 1,000 mg/L feed. Improving the element's efficiency alone is therefore unlikely to decrease the overall system SEC significantly. However, element upgrades that enable higher pressure operation, or increase water recovery, could promote significant energy savings at other components.

This work can guide new developments to decrease the impact of POU RO devices on scarce energy and groundwater resources in countries such as India, where they are increasingly used.

Acknowledgements

We thank Ben Katz for providing access to his dynamometer and helping to characterize the motor. We also thank Dr. Sathish Kumar and the team at Eureka Forbes Ltd for providing the point-of-use purifier that was evaluated in this study, as well as guidance on the POU RO market.

This work was supported by the Abdul Latif Jameel Water and Food Systems Lab (J-WAFS) at MIT. Additionally, we acknowledge the support of the Natural Sciences and Engineering Research Council of Canada (NSERC), funding reference number PGSD3-516795-2018.

Cette recherche a été financé par le Conseil de recherches en sciences naturelles et en génie du Canada (CRSNG), numéro de référence PGSD3-516795-2018.

Symbols

\dot{m}	—	Mass flow rate
\dot{W}_{least}	—	Least work of separation
\dot{W}_{sep}	—	Work of separation
A_m	—	Membrane permeability
b	—	Molality
h	—	Specific enthalpy
I	—	Motor current draw
J_w	—	Permeate flux
k_T	—	Motor torque constant
k_v	—	Motor velocity constant
L	—	Membrane length
M	—	Molar mass
P	—	Press
Q	—	Volumetric flow rate
R	—	Gas constant

r	—	Recovery ratio
R_m	—	Motor winding resistance
S^m	—	Membrane area
s	—	Specific entropy
T	—	Temperature
V	—	Motor voltage
W	—	Membrane width
w	—	Mass fraction

Greek

η_{II}	—	Second law efficiency
γ	—	Mean molal activity
μ	—	Chemical potential energy
ω	—	Motor speed
\dot{E}	—	Exergy
φ	—	Osmotic coefficient
ρ	—	Density
τ	—	Motor torque
ξ	—	Specific exergy

Subscripts and superscripts

*	—	Restricted dead state
0	—	Global dead state
b	—	Brine
d	—	Destroyed
e	—	RO membrane element
f	—	Feed
fr	—	Flow restrictor
i	—	i -th stream or component
p	—	Product
s	—	Process stream
w	—	Work

References

- [1] The International Bank for Reconstruction and Development/ The World Bank, Deep Wells and Prudence: Towards Pragmatic Action for Addressing Groundwater Overexploitation in India, 2010.
- [2] N.C. Wright, A.G. Winter V, Justification for community-scale photovoltaic-powered electro dialysis desalination systems for inland rural villages in India, *Desalination*, 352 (2014) 82–91.
- [3] Bureau of Indian Standards, IS 10500 – Drinking Water Specification, 2012.
- [4] Bureau of Indian Standards, Report of Testing of Piped Drinking Water Samples from 20 Capital Cities and Delhi, 2019.
- [5] R. Ghosh, A. Kansal, S. Aghi, Implications of end-user behaviour in response to deficiencies in water supply for electricity consumption – A case study of Delhi, *J. Hydrol.*, 536 (2016) 400–408.
- [6] M. Elimelech, W.A. Phillip, The future of seawater desalination: energy, technology, and the environment, *Science*, 333 (2011) 712–717.
- [7] Massachusetts Institute of Technology Comprehensive Initiative on Technology Evaluation, Household Water Filter Evaluation Project Report, 2015.
- [8] Chennai Metropolitan Water Supply and Sewerage Board, Republic of India Preparatory Survey on Chennai Seawater Desalination Plant Project – Final Report, 2017, pp. 3–44.
- [9] W. Arras, N. Ghaffour, A. Hamou, Performance evaluation of BWRO desalination plant – a case study, *Desalination*, 235 (2009) 170–178.
- [10] M. Alghoul, P. Poovanaesvaran, K. Sopian, M. Sulaiman, Review of brackish water reverse osmosis (BWRO) system designs, *Renewable Sustainable Energy Rev.*, 13 (2009) 2661–2667.
- [11] M. Al-Obaidi, A. Alsarayreh, A. Al-Hroub, S. Alsadaie, I. Mujtaba, Performance analysis of a medium-sized industrial reverse osmosis brackish water desalination plant, *Desalination*, 443 (2018) 272–284.
- [12] T. Gleeson, Y. Wada, M.F.P. Bierkens, L.P.H. van Beek, Water balance of global aquifers revealed by groundwater footprint, *Nature*, 488 (2012) 197–200.
- [13] Frost & Sullivan, Indian Water Purifiers Market (FY2018), 2018.
- [14] H. Elfil, A. Hamed, A. Hannachi, Technical evaluation of a small-scale reverse osmosis desalination unit for domestic water, *Desalination*, 203 (2007) 319–326.
- [15] S. Thampy, G.R. Desale, V.K. Shahi, B.S. Makwana, P.K. Ghosh, Development of hybrid electro dialysis-reverse osmosis domestic desalination unit for high recovery of product water, *Desalination*, 282 (2011) 104–108.
- [16] Eureka Forbes Ltd., Dr. Aquaguard Magna RO Purifier. Available at: <https://www.eurekaforbes.com/water-purifiers/dr-aquaguard-magna-nxt-hd-ro-uv> (Accessed: 2019-01-05).
- [17] Pentair Filtration & Process, TLCTM Thin Layer Composite Residential Membranes. Available at: <https://www.pentair.com/content/dam/extranet/brochures-and-catalogs/waterpurification/tlc/4001415-rev-d-mr14.pdf> (Accessed: 2019-09-21).
- [18] Applied Membranes Inc., DOW FilmTec™ BW60-1812-75 Membrane Specifications. Available at: https://www.appliedmembranes.com/media/wysiwyg/pdf/membranes/bw60-181275_membrane_specifications.pdf (Accessed: 2019-09-20).
- [19] E.W. Tow, D.M. Warsinger, A.M. Trueworthy, J. Swaminathan, G.P. Thiel, S.M. Zubair, A.S. Myerson, J.H. Lienhard V, Comparison of fouling propensity between reverse osmosis, forward osmosis, and membrane distillation, *J. Membr. Sci.*, 556 (2018) 352–364.
- [20] M. Freire-Gormaly, A. Bilton, Impact of intermittent operation on reverse osmosis membrane fouling for brackish groundwater desalination systems, *J. Membr. Sci.*, 583 (2019) 220–230.
- [21] C. Tzotzi, T. Pahiadaki, S. Yiantsios, A. Karabelas, N. Andritsos, A study of CaCO₃ scale formation and inhibition in RO and NF membrane processes, *J. Membr. Sci.*, 296 (2007) 171–184.
- [22] Y.D. Ahdab, Desalination of Brackish Groundwater in the United States: Minimum Energy Requirements, Master's Thesis, Massachusetts Institute of Technology, 2017.
- [23] C.P. Koutsou, S.G. Yiantsios, A.J. Karabelas, A numerical and experimental study of mass transfer in spacer-filled channels: effects of spacer geometrical characteristics and Schmidt number, *J. Membr. Sci.*, 326 (2009) 234–251.
- [24] B. Katz, Build Its in progress: Motor Dyno. Available at: <http://build-its-inprogress.blogspot.com/2016/10/motor-dyno-updates-first-tests.html> (Accessed: 2018-09-05).
- [25] K.H. Mistry, R.K. McGovern, G.P. Thiel, E.K. Summers, S.M. Zubair, J.H. Lienhard V, Entropy generation analysis of desalination technologies, *Entropy*, 13 (2011) 1829–1864.
- [26] B.A. Qureshi, S.M. Zubair, Exergetic analysis of a brackish water reverse osmosis desalination unit with various energy recovery systems, *Energy*, 93 (2015) 256–265.
- [27] A.M. Blanco-Marigorta, A. Lozano-Medina, J.D. Marcos, A critical review of definitions for exergetic efficiency in reverse osmosis desalination plants, *Energy*, 137 (2017) 752–760.
- [28] J.I. Partanen, Mean activity coefficients and osmotic coefficients in dilute aqueous sodium or potassium chloride solutions at temperatures from 0 to 70°C, *J. Chem. Eng. Data*, 61 (2016) 286–306.
- [29] Hydranautics, Hydranautics Design Limits. Available at: http://membranes.com/docs/trc/Dsgn_Lmt.pdf (Accessed: 2019-09-25).
- [30] LANXESS Lewabrane, Guidelines for the Design of Reverse Osmosis Membrane Systems. Available at: http://membranes.com/docs/trc/Dsgn_Lmt.pdf (Accessed: 2019-09-25).
- [31] L.G. Chem, Nano H₂O₂ Membranes, Residential Reverse Osmosis (RO) Element. Available at: <https://watertechgroup.com/images/Datasheets/ro-nano-uf/lg-membrane/>

- Igresidential/Water-Tech---LG-Chem-Residential-RO-Membranes.pdf (Accessed: 2019-09-21).
- [32] T. Qiu, P.A. Davies, Comparison of configurations for high-recovery inland desalination systems, *Water*, 4 (2012) 690–706.
- [33] D.M. Warsinger, E.W. Tow, K.G. Nayar, L.A. Maswadeh, J.H. Lienhard V, Energy efficiency of batch and semi-batch (CCRO) reverse osmosis desalination, *Water Res.*, 106 (2016) 272–282.
- [34] J.R. Werber, A. Deshmukh, M. Elimelech, Can batch or semi-batch processes save energy in reverse-osmosis desalination?, *Desalination*, 40 (2017) 109–122.
- [35] Q.J. Wei, C.I. Tucker, P.J. Wu, A.M. Truworthly, E.W. Tow, J.H. Lienhard V, Batch Reverse Osmosis: Experimental Results, Model Validation, and Design Implications, Membrane Technology Conference & Exposition, (New Orleans, LA), American Membrane Technology Association, 2019.
- [36] M. Chaturvedi, T. Ghosh, L. Bhandari, Assessing Income Distribution at the District Level for India Using Nighttime Satellite Imagery, *Proceedings of the Asia-Pacific Advanced Network*, 32 (2011) 192.
- [37] Global Water Intelligence. Available at: <https://www.desaldata.com/> (Accessed: 2019-09-11).
- [38] MATLAB, version 9.6.0 (R2019a), Natick, Massachusetts: The MathWorks Inc., 2010.
- [39] K.H. Mistry, J.H. Lienhard V, Effect of nonideal solution behavior on desalination of a sodium chloride (NaCl) solution and comparison to seawater, *Energy*, 6 (2012) 1509–1523.
- [40] G. Kortum, *Treatise on Electrochemistry*, Elsevier Publishing Company, 1965.
- [41] R.W. Potter, D.L. Brown, The Volumetric Properties of Aqueous Sodium Chloride Solution from 0 to 500°C at Pressures up to 2,000 bars Based on Regression of Available Data in the Literature, United States Department of the Interior, 1977.

Appendix

A1. Comparing the energy consumption and recovery of POU RO systems to the Minjur desalination plant

In Table A1, we estimate the aggregate daily feed intake, product output, and energy consumption for all point-of-use (POU) reverse osmosis (RO) systems in the city of Delhi for the year 2018. These estimates are derived for high (HIG), middle (MIG), low (LIG) income group households, as defined by the Delhi Development Authority. Device usage statistics were collected by Ghosh et al. [5] for each income group, while total households in the same categories were taken from Chaturvedi et al. [36]. The assumed recovery ratio and energy consumption was taken from manufacturer specifications [16].

Table A1
Estimating the scale of water production and energy consumption of POU RO devices in Delhi

	HIG	MIG	LIG	Total
Number of households in Delhi	156,518	486,945	2,967,884	3,611,347
Percentage with device (%)	77	44	27	
Mean household size	4.12	4.06	4.25	
Average feed consumption (L/person-d)		9.4		
Specific energy consumption (kWh/m ³)		3		
Recovery ratio (%)		25		
Feed intake (× 10 ⁶ L/d)	4.7	8.2	32.0	44.9
Product output (× 10 ⁶ L/d)	1.2	2.0	8.0	11.2
Energy consumption (MWh/d)	3.5	6.1	24.0	33.7

Fig. 1 in the main text then compares these estimates to data published for the Minjur seawater desalination plant. It has a nominal capacity of 100,000 m³/d, consumes 2.9 kWh/m³ of produced water [37], and operates at 45% recovery [8].

A2. Experimental measurements

Table A2 provides the raw data collected in the evaluation of the point-of-use RO purifier. Current refers to the current draw of the pump motor, and Time refers to the duration over which product and brine were collected for each test.

A3. Motor characterization

Dynamometer measurements were used to estimate the torque constant k_T (N-m/A), speed constant k_V (V-s/rad) and winding resistance R_m (Ohms). The slope and intercepts of the measured torque-current and speed-torque curves were used to solve these constants (Fig. A3). The relevant linear relationships are:

$$k_T = \frac{d\tau}{dI} \quad (A1)$$

$$k_V = \frac{V}{\omega_{\max}}, \text{ and} \quad (A2)$$

$$\frac{R_m}{k_V k_T} = -\frac{d\omega}{d\tau} \quad (A3)$$

where the motor torque is τ (N-m), I is the current (A), and ω_{\max} is the no-load speed (rad/s) at voltage V (V). MATLAB was used to perform the linear regression and plot the prediction intervals that are shown [38].

A4. Least work of separation derivation

The least work corresponds to the power required to separate the feed stream into a diluted product stream, and a concentrated brine stream at the same temperature and pressure as the feed. It is derived on a mole basis from the first and second laws of thermodynamics in [39] to be:

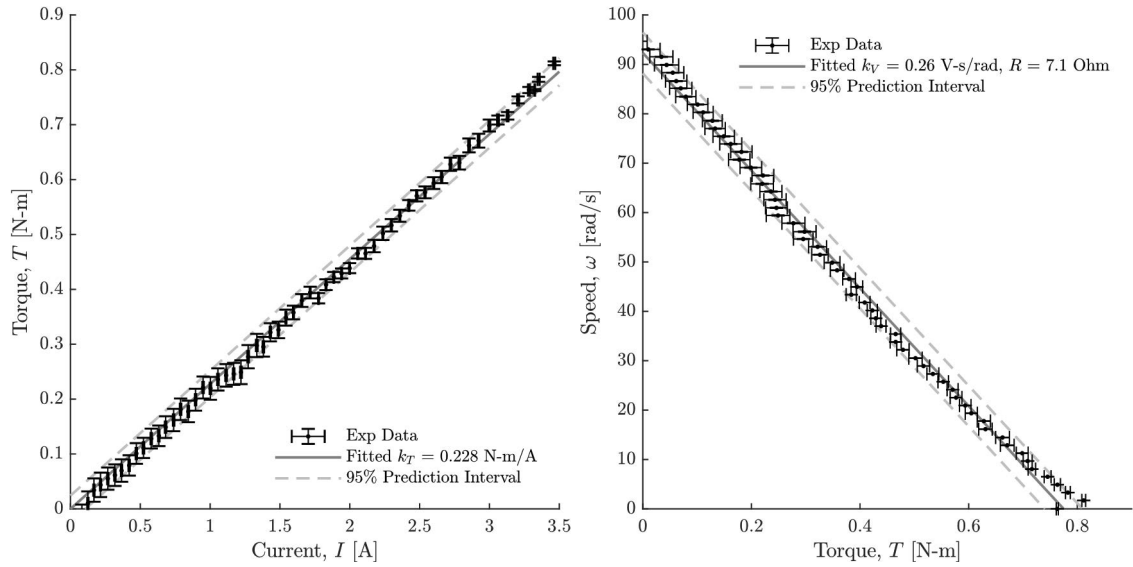


Fig. A3. k_T equals the slope of measured torque vs. current (left). k_V and R_m were estimated from the y-intercept and slope of the measured speed vs. torque (right). The fitted models [Eqs. (19)–(21)] match all experimental data within error. Each experimental data point represents the mean of 600 measurements. The error-bars on experimental data span the 95% confidence interval of the mean.

$$\begin{aligned} \dot{W}_{\text{least}} = & \left[\dot{n}_{\text{H}_2\text{O}} RT \ln(a_{\text{H}_2\text{O}}) + \dot{n}_{\text{NaCl}} RT \ln(a_{\text{NaCl}}) \right]_p \\ & + \left[\dot{n}_{\text{H}_2\text{O}} RT \ln(a_{\text{H}_2\text{O}}) + \dot{n}_{\text{NaCl}} RT \ln(a_{\text{NaCl}}) \right]_b \\ & - \left[\dot{n}_{\text{H}_2\text{O}} RT \ln(a_{\text{H}_2\text{O}}) + \dot{n}_{\text{NaCl}} RT \ln(a_{\text{NaCl}}) \right]_f \end{aligned} \quad (\text{A4})$$

The molar flow rates of water and salt are $n_{\text{H}_2\text{O}}$ and n_{NaCl} (mol/s), respectively. R is the gas constant (J/mol·K), T is the temperature (K), and the product, brine, and feed streams are differentiated by subscripts p , b , and f , respectively. The water and salt mole balances

$$\dot{n}_{\text{H}_2\text{O},f} = \dot{n}_{\text{H}_2\text{O},p} + \dot{n}_{\text{H}_2\text{O},b} \quad \text{and} \quad (\text{A5})$$

$$\dot{n}_{\text{NaCl},f} = \dot{n}_{\text{NaCl},p} + \dot{n}_{\text{NaCl},b} \quad (\text{A6})$$

are substituted into the above equation to give:

$$\begin{aligned} \dot{W}_{\text{least}} = & \left[\dot{n}_{\text{H}_2\text{O},p} RT \ln\left(\frac{a_{\text{H}_2\text{O},p}}{a_{\text{H}_2\text{O},f}}\right) + \dot{n}_{\text{NaCl},p} RT \ln\left(\frac{a_{\text{NaCl},p}}{a_{\text{NaCl},f}}\right) \right] \\ & + \left[\dot{n}_{\text{H}_2\text{O},b} RT \ln\left(\frac{a_{\text{H}_2\text{O},b}}{a_{\text{H}_2\text{O},f}}\right) + \dot{n}_{\text{NaCl},b} RT \ln\left(\frac{a_{\text{NaCl},b}}{a_{\text{NaCl},f}}\right) \right] \end{aligned} \quad (\text{A7})$$

The activities are expressed in terms of the osmotic coefficients ϕ and mean molal activity coefficients γ using:

$$\ln(a_{\text{H}_2\text{O}}) = -\nu\phi b_{\text{NaCl}} M_{\text{H}_2\text{O}} \quad \text{and} \quad (\text{A8})$$

$$\ln(a_{\text{NaCl}}) = -\nu \ln(\gamma b_{\text{NaCl}}) \quad (\text{A9})$$

where $\nu = 2$ because one mole of sodium chloride dissolves to form two moles of ions. These thermodynamic

properties were taken from [28] at atmospheric pressure, and the temperature of the feed solution. Note that:

$$\frac{\dot{n}_{\text{NaCl}}}{\dot{n}_{\text{H}_2\text{O}}} = b_{\text{NaCl}} M_{\text{H}_2\text{O}} \quad (\text{A10})$$

where b_{NaCl} is the molality of NaCl and $n_{\text{H}_2\text{O}}$ (kg/mol) is the molar mass of water. Substituting Eqs. (26)–(28) into Eq. (25) gives the final expression.

$$\begin{aligned} \dot{W}_{\text{least}} = & 2\dot{m}_{\text{H}_2\text{O},p} RT \left[-b_{\text{NaCl},p} \phi_p + b_{\text{NaCl},f} \phi_f + b_{\text{NaCl},p} \ln\left(\frac{\gamma_p b_{\text{NaCl},p}}{\gamma_f b_{\text{NaCl},f}}\right) \right] \\ & + 2\dot{m}_{\text{H}_2\text{O},b} RT \left[-b_{\text{NaCl},b} \phi_b + b_{\text{NaCl},f} \phi_f + b_b \ln\left(\frac{\gamma_b b_{\text{NaCl},b}}{\gamma_f b_{\text{NaCl},f}}\right) \right] \end{aligned} \quad (\text{A11})$$

where the mass flow rate of water $\dot{m}_{\text{H}_2\text{O}}$ (kg/s) in each stream is:

$$\dot{m}_{\text{H}_2\text{O}} = \dot{n}_{\text{H}_2\text{O}} M_{\text{H}_2\text{O}} \quad (\text{A12})$$

A5. Molality, molarity, and density relations

Solution molarities c (mol/L) were calculated using the Onsager–Falkenhagen relation:

$$\Lambda = \Lambda_0 - (K_1 \Lambda_0 + K_2) \frac{\sqrt{c}}{1 + K_0 a \sqrt{c}} \quad (\text{A13})$$

where the specific conductance Λ (S·cm²/mol) is related to the conductivity measurements σ (uS/cm) through:

Table A2
Results from experimental evaluation of a commercial point-of-use RO desalination system

Test	Feed cond. ($\mu\text{S}/\text{cm}$)	Temp. ($^{\circ}\text{C}$)	Current ^a (A)	Pressure (psi)		Time (s)	Mass ^b (g)		Conductivity ($\mu\text{S}/\text{cm}$)	
				Feed	Back		Prod.	Brine	Prod.	Brine
				$\pm 1\%$	$\pm 0.1^{\circ}\text{C}$		± 0.01 A	± 1 psi	± 1 s	± 2 g
1	1,329	22.0	0.30	10	6.0 \pm .1	40	90	1,308	170	1,333
2	1,327	22.4	0.40	20	15.8 \pm .2	50	115	1,473	116	1,356
3	1,316	22.2	0.52	30	28.0 \pm .5	60	163	1,603	83	1,383
4	1,332	22.7	0.61	40	38.8 \pm .1	55	187	1,343	69	1,430
5	1,327	23.6	0.69	50	47.1 \pm .3	50	203	1,157	52	1,474
6	1,318	23.3	0.77	60	58.3 \pm .3	45	218	943	47	1,531
7	1,315	24.0	0.85	71	68.0 \pm .3	45	245	851	45	1,590
8	1,310	24.3	0.93	81	78.7 \pm .3	45	268	736	44	1,690
9	1,219	24.2	1.01	91	91.4 \pm .2	45	284	364	59	2,340
10	1,991	22.8	0.29	10	4.6 \pm .3	30	87	1,054	– ^c	1,996
11	1,997	23.3	0.40	20	16.7 \pm .1	45	106	1,334	127	2,017
12	2,035	23.5	0.51	30	28.4 \pm .3	45	134	1,213	150	2,117
13	2,028	23.7	0.60	40	38.0 \pm .1	45	158	1,133	113	2,167
14	2,031	23.9	0.68	50	48.5 \pm .3	45	184	1,028	94	2,236
15	2,021	24.0	0.77	60	58.5 \pm .3	45	208	930	85	2,317
16	2,010	24.2	0.85	71	68.4 \pm .2	45	232	832	91	2,412
17	2,001	24.3	0.93	81	80.8 \pm .1	45	257	686	83	2,590
18	1,991	24.7	0.99	91	89.9 \pm .2	45	269	410	101	3,180
19	3,514	25.0	0.39	20	16.5 \pm .3	45	94	1,353	983	3,515
20	3,493	24.9	0.50	30	28.3 \pm .1	45	112	1,259	893	3,565
21	3,507	24.9	0.59	40	37.9 \pm .2	45	134	1,180	416	3,647
22	3,502	24.9	0.70	50	49.0 \pm .3	45	162	1,058	262	3,763
23	3,497	24.9	0.79	60	59.0 \pm .5	50	193	1,035	216	3,875
24	3,487	25.0	0.87	71	69.5 \pm .2	45	208	880	197	4,018
25	3,474	25.0	0.94	81	80.0 \pm .6	45	228	750	187	4,209
26	3,408	24.9	1.00	91	90.4 \pm .3	45	239	439	224	5,019

^aPump voltage was held constant at 24.1 ± 0.1 V.

^bMass collected includes product and brine container masses of 86 ± 1 g and 161 ± 1 g, respectively.

^cThe product volume collected in Test 10 was insufficient for conductivity measurements.

Table A3
Onsager/Falkenhagen constants for NaCl solutions [40]

Temp. ($^{\circ}\text{C}$)	Λ_0	a	K_0	K_1	K_2
20	113.76	4	0.3276	0.2269	53.48
25	126.45	4	0.3286	0.2289	60.32

$$\sigma = (1000 \mu\text{S}/\text{S}) \Lambda c \quad (\text{A14})$$

The coefficients K_0 – K_3 and a are tabulated for 20°C and 25°C (Table A3), and linear interpolation was applied to calculate Λ at intermediate temperatures.

Conversion from molarity to molality b (mol/kg) was performed using:

$$b = \frac{c}{\frac{\rho}{1000} - cM_{\text{NaCl}}} \quad (\text{A15})$$

where the density of the solution ρ (kg/m^3) was itself correlated to molality through:

$$\rho = \rho_{\text{H}_2\text{O}} \frac{1 + bM_{\text{NaCl}}}{1 + A_0 b \rho_{\text{H}_2\text{O}} + B_0 b^{3/2} \rho_{\text{H}_2\text{O}} + C_0 b^2 \rho_{\text{H}_2\text{O}}} \quad (\text{A16})$$

where, M_{NaCl} (kg/mol) is the molar mass of sodium chloride, $\rho_{\text{H}_2\text{O}} = 997.047 \text{ kg}/\text{m}^3$ is density of pure water at 25°C , and the empirical coefficients are $A_0 = 16.62 \times 10^{-6}$, $B_0 = 1.773 \times 10^{-6}$, and $C_0 = 0.098 \times 10^{-6}$ [41].

The average total (water and salt) mass flow rate m (kg/s) for each stream is taken as the ratio of the measured mass over time. The associated volumetric flow rate is:

$$Q = \frac{m}{\rho} \quad (\text{A17})$$

The mass flow rate of only water $\dot{m}_{\text{H}_2\text{O}}$ (kg/s) in the stream is subsequently.

$$\dot{m}_{\text{H}_2\text{O}} = \rho_{\text{H}_2\text{O}} Q \quad (\text{A18})$$